In Vivo Imaging of the Mouse Model of X-Linked Juvenile Retinoschisis with Fourier Domain Optical Coherence Tomography

Jing Xu,[1] *Laurie L. Molday,*[2] *Robert S. Molday,*[2] *and Marinko V. Sarunic*[1]

Purpose. The purpose of this study was to investigate Fourier domain optical coherence tomography (FD OCT) as a noninvasive tool for retinal imaging in the *Rs1h*-knockout mouse (model for X-linked juvenile retinoschisis).

Methods. A prototype spectrometer-based FD OCT system was used in combination with a custom optical beam–scanning platform. Images of the retinas from wild-type and *Rs1h*-knockout mice were acquired noninvasively with FD OCT with the specimen anesthetized. At the completion of the noninvasive FD OCT imaging, invasive retinal cross-sectional images (histology) were acquired from a nearby region for comparison to the FD OCT images.

Results. The retinal layers were identifiable in the FD OCT images, permitting delineation and thickness measurement of the outer nuclear layer (ONL). During FD OCT in vivo imaging of the *Rs1h*-knockout mouse, holes were observed in the inner nuclear layer (INL), and retinal cell disorganization was observed as a change in the backscattering intensity profile. Comparison of the ONL measurements acquired noninvasively with FD OCT to measurements taken using histology at nearby locations showed a degeneration of roughly 30% of the ONL by the age of 2 months in *Rs1h*-knockout mice relative to wild-type.

Conclusions. FD OCT was demonstrated to be effective for noninvasive imaging of retinal degeneration and observation of retinal holes in *Rs1h*-knockout mice. (*Invest Ophthalmol Vis Sci.* 2009;50:2989–2993) DOI:10.1167/iovs.08-2542

Significant inroads have been made into human retinal imaging by Fourier domain optical coherence tomography (FD OCT).[1–8] As the FD OCT imaging modality is gaining wider acceptance for its diagnostic utility, the investigation of FD OCT as a tool for basic visual science with animal models of retinal degeneration is also generating increasing interest. In contrast to human clinical imaging where only noninvasive imaging modalities can be used, research involving animal models can use invasive histology on enucleated eyes, permitting confocal imaging of immunologic stained sections to enhance the contrast of retinal features. Noninvasive imaging with FD OCT has the distinct advantage of facilitating longitudinal studies on the time course of diseases and has the potential to accelerate basic medical research by significantly reducing the number of animals required. Furthermore, noninvasive imaging with FD OCT has the ability to identify abnormal structural morphology in vivo, removing concerns of potential tissue processing artifacts introduced by histology.

Attempts to investigate retinal degeneration in mice with early time domain OCT systems were hampered by low resolution and slow image acquisition.[9–11] Investigation of retinal degeneration with FD OCT in rodents is at an early stage, and to date only wild-type (WT) specimens and simple models of retinal degeneration have been imaged.[12–14] Two techniques of focusing the light on the rodent retina have been investigated. In one approach,[13] a collimated beam was used, relying on the refractive elements of the mouse eye to focus the beam on a spot on the retina. In another approach,[12,14] a focused beam was used in conjunction with a contact lens to cancel out the refraction by the cornea. Irrespective of the technique used, the retinal layers were identifiable by their relative scattering intensity, similar to human retinal imaging. An investigation of FD OCT for a time course study of retinal degeneration in the *rd1* mouse was presented by Kim et al.,[14] who used a pulsed femtosecond titanium/sapphire laser providing 110 nm of bandwidth at an 800-nm center. Degeneration was quantified by comparing the ratio of the thickness of the outer retina (including the layers from the outer plexiform layer [OPL] to the outer segment [OS] of the photoreceptor layer) with the thickness of the whole retina (including the layers from the nerve fiber layer [NFL] to the OS).

In this study we built on the existing literature studying FD OCT as a noninvasive imaging modality for the study of retinal degeneration in mice in vivo. The mouse model for X-linked juvenile retinoschisis (RS), a form of genetic retinal degeneration in males, was investigated in this FD OCT research application. These knockout mice are deficient in the *Rs1h* gene, the orthologue to the *RS1* gene in humans, and their eyes have been shown through histology to be characterized by holes in the inner nuclear layer (INL),[15] disorganization of the retinal cell layers, and slow progressive degeneration of the photoreceptors. We present a comparison of noninvasive retinal imaging in *Rs1h*-knockout (KO) and WT mice acquired with the FD OCT with invasive histologic sections. Qualitatively, disorganization of the retinal morphology associated with the *Rs1h*-KO mouse was observed with FD OCT, as well as the holes in the INL characteristic of RS. The application of FD OCT to provide quantitative measurements was also investigated. The metric used to quantify the amount of retinal degeneration was the thickness of the outer nuclear layer (ONL) which thins with increasing age in *Rs1h* mice. Two-dimensional maps of the ONL thickness were extracted from the FD OCT volume data acquired on WT and *Rs1h*-KO mice. From the standpoint of

From the [1]School of Engineering Science, Simon Fraser University, Burnaby, British Columbia, Canada; and the [2]Department of Biochemistry and Molecular Biology, Centre for Macular Research, University of British Columbia, Vancouver, British Columbia, Canada.

Supported by Natural Sciences and Engineering Research Council (NSERC) Discovery Grant 31-611498 (MVS), a Michael Smith Foundation for Health Research (MSFHR) Career Investigator Award (MVS), National Eye Institute Grant EY 02422 (RSM), a Foundation Fighting Blindness Grant (RSM), and Canadian Institutes for Health Research (CIHR)/FFB Grant RMF-92101 (RSM, MVS).

Submitted for publication July 8, 2008; revised December 9 and 16, 2008; accepted April 16, 2009.

Disclosure: **J. Xu**, None; **L.L. Molday**, None; **R.S. Molday**, None; **M.V. Sarunic**, None

The publication costs of this article were defrayed in part by page charge payment. This article must therefore be marked "*advertisement*" in accordance with 18 U.S.C. §1734 solely to indicate this fact.

Corresponding author: Marinko V. Sarunic, Simon Fraser University, 8888 University Drive, Burnaby, BC V5A 1S6, Canada; msarunic@sfu.ca.

evaluating a research tool, the FD OCT system used in this study used a cost-effective and portable continuous superluminescent diode (SLED) light source, nominally one tenth the cost of an exotic femtosecond laser, and a custom sample arm constructed from bulk achromatic lenses.

METHODS

FD OCT

A prototype FD OCT system was constructed for mouse retinal imaging. The standard interferometer topology used in this report, presented in Figure 1, consisted of a source, fiber coupler, and custom spectrometer–based detection. The SLED source (Superlum, Moscow, Russia) had a central wavelength of 826 nm and a spectral bandwidth full width at half maximum (FWHM) of 72 nm. The corresponding transform limited axial resolution was nominally 4 μm in tissue. During animal imaging, the optical power output from the source was reduced to 770 μW, the ANSI limit for maximum exposure of the retina to continuous light at this wavelength.[16] The interferometer was constructed from a 2 $\times$ 2 fiber coupler (AC Photonics, Santa Clara, CA) with an 80/20 splitting ratio. This configuration was used to provide 20% of the source light to the sample arm, but in the reverse direction, 80% of the collected light was directed to the detector to optimize the optical signal. The reference arm consisted simply of a collimating lens, attenuator, and mirror. Dispersion was corrected purely through numerical techniques,[4] and no additional optics were included in the reference arm. The sample arm consisted of a collimating lens followed by a pair of galvanometer mounted mirrors for raster scanning control of the beam. The beam expander and objective lenses after the scanning mirrors, as indicated in Figure 1, were constructed from antireflection-coated achromatic lenses. The calculated spot size given the optical configuration was nominally 13 μm with a depth of focus of 350 μm, designed to provide high-resolution lateral images, while spanning the full retinal thickness. The sample arm optics were mounted on a slit lamp biomicroscope stage for positioning of the beam relative to the mouse eye.

The high-speed spectrometer used was a custom design constructed with a 1200 l/mm transmission diffraction grating. The detector was a 1024-element, high-speed camera (Spyder3, GigE; Dalsa, Waterloo, ON, Canada) with 14-μm^2 pixels. The camera can operate at a maximum line rate of 68 kHz, but was typically reduced to 20 kHz for imaging. Data acquisition was performed with custom software written in C++ for rapid frame grabbing, processing, and display of two-dimensional images. Processing performed in real time included resampling of the interferometric data from linearly sampled in wavelength space to linear sampling in wavenumber space, fast Fourier transform (FFT), and image contrast and brightness. Dispersion compensation was also performed by the software up to the third term, but was limited to real-time display of nominally 30 frames per second under imaging conditions of 512 lines per frame.

FD OCT Mouse Imaging

Although the FD OCT imaging is noninvasive, to keep the mice still during imaging they were anesthetized with an intraperitoneal injection of ketamine and xylazine mixture (0.1 mL per 10 g body weight).

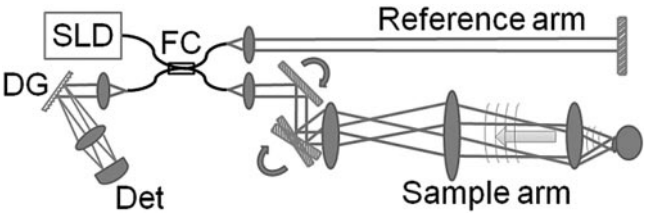

FIGURE 1. The FD OCT interferometric setup used to image the mouse retina.

After anesthetization, the mouse was placed gently on a heating pad to maintain warmth, and simple manual manipulation was used to rest the head of the mouse in an orientation where the angle of the eye was properly coupled to the optical beam. The pupils were dilated with a topical solution (atropine sulfate 1%). Refraction of light at the cornea was cancelled by placing a flat coverslip generously coated with a generic artificial tear gel over the eye. Alignment of the optical system to the mouse retina required several minutes and was followed by rapid acquisition of data, requiring nominally 5 seconds per volume. During imaging, the software displayed the FD OCT B-scans at ~30 frames/s. Registration of the location of the B-scan within the two-dimensional surface of the retina was performed by switching the display mode to a high-speed (60-kHz line rate), low-sampling-density area scan, representing a reconstructed fundus type image. All mouse handling adhered to the ARVO Statement for the Use of Animals in Ophthalmic and Vision Research, and the experiments were performed under protocols compliant with the Canadian Council on Animal Care with the approval of the University Animal Care Committee at SFU.

The ONL thickness measurements were extracted by postprocessing saved data. A fundus-type image of the mouse retina was reconstructed by using the FD-OCT volumetric data[7] and was used to register the location of the ONL thickness measurement 400 μm from the optic nerve head where the retinal layers were of nominally constant cross section. The ONL boundaries were delineated by manually placing points at the boundary between layers and fitting a low-order polynomial to the points with a commercial mathematical software package (MatLab; The MathWorks, Natick, MA). The ONL thickness was subsequently measured along a line in the image and was calculated perpendicular to the curvature of the retina by using Snell's law calculations to account for refractive index changes.[17,18] The estimated average refractive index of the retina was $n_{retina} = 1.38$. The recorded ONL thickness for a given eye was calculated as the mean of three adjacent depth profile frames to average out human error in delineation of the ONL boundaries. Automated computer segmentation of the depth profiles using advanced image processing algorithms is under development to complement the FD-OCT image acquisition and reduce interobserver variation. After the noninvasive FD OCT measurement, the mice were euthanatized, and the eyes were enucleated for histology.

Histology

Immediately after FD OCT measurements (hours), the mice were killed, and the eyes were enucleated and fixed in 4% paraformaldehyde in 0.1 M phosphate buffer (pH 7.2) for 15 hours. After fixation, the samples were washed and frozen in OCT compound, cut into 12-μm sections and stained with DAPI nuclear stain. The retina sections were visualized with a fluorescence microscope (Axioplan; Carl Zeiss Meditec, Inc., Dublin, CA), and the ONL thickness was measured by counting the number of nuclei at five locations in the DAPI-stained histologic sections.

RESULTS

Correlation of FD OCT Depth Profiles with Histologic Sections

Cross-sectional depth profiles in FD OCT consist of alternating bright and dark regions, corresponding to the backscattering intensity of the various retinal layers. The retinal layers can be identified in the FD OCT images through comparison with a histologic section, as shown in Figures 2a and 2b. The thickness of the outer nuclear layer (ONL) was measured as the distance of the dark band between the bright lines constituting the outer plexiform layer (OPL) and the inner segment (IS) of the photoreceptor layer. To measure the thickness of the ONL, each FD OCT image was first manually segmented by selecting points on each curved boundary and fitting them to a low

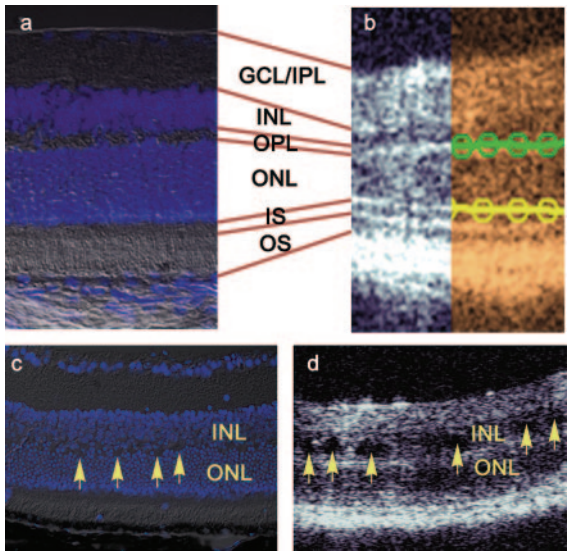

FIGURE 2. Comparison of the WT mouse retinal layers observed in (**a**) a DAPI-stained histologic section merged with DIC to (**b**) noninvasive FD OCT. The retinal layers were segmented manually and fit to a fourth-order polynomial that was subsequently used for the thickness measurement. *Arrows*: holes observed in the INL of a (**c**) DAPI-stained section and (**d**) an FD OCT image of the retina of a 2-month-old *Rs1h*-KO mouse. GCL, ganglion cell layer; IPL, inner plexiform layer; OPL, outer plexiform layer, ONL, outer nuclear layer; IS, inner segment; OS, outer segment.

order polynomial, as described in the Methods section. In Figure 2b, the OPL/ONL boundary is indicated by the green line fit to the manually selected points represented by the circles. The ONL/IS boundary was similarly delineated, and is represented in yellow.

Retinal Structure in the *Rs1h*-KO Mice

In the FD OCT images, irregularities in the retinal layer structure of the *Rs1h*-KO mouse were observed relative to the WT. A sample FD OCT image of an *Rs1h*-KO mouse is shown adjacent to a histologic section in Figures 2c and, 2d. The OPL layer and the IS/OS photoreceptor layers appeared thicker in the FD OCT image due to poorly defined ONL boundaries. In the DAPI-stained histologic image, the OPL between the ONL and INL was not well resolved. Characteristic to RS, holes, or cavities were also observed in the INL layers in the FD OCT images and also in the histologic sections.

ONL Thickness Measurements with FD OCT and Histology

For this study, we compared measurements of the ONL thickness in *Rs1h*-KO mice with those of their WT counterparts. The ONL thickness was measured in both eyes of each specimen used. The control group consisted of six WT mice for the FD OCT measurement, corresponding to a sample size of $n = 12$ eyes. The control group for the DAPI-stained histology control group consisted of five specimens, corresponding to a sample size of 10. Two mice were used for each age group of *Rs1h*-KO mice investigated, making a sample size of $n_{\mathrm{RS1hXmo}} = 4$ eyes (X represents the age of the specimen in months). Three ages of *Rs1h*-KO mice were used in this study: 2, 10, and 15 months. The reported ONL thicknesses represent the average and SD of n measurements from each group.

Examples of the fundus reconstruction and depth profile images acquired with the FD OCT are presented alongside DAPI-stained histology in Figure 3. The fundus image represents a volumetric data set; a FD-OCT depth scan of information is contained in each horizontal line.

The numerical results of the ONL thickness measurements comparing FD-OCT to DAPI-stained histology are summarized in Table 1. The ratio was calculated using the average ONL thickness measurement from each *Rs1h*-KO group and dividing it by that of the corresponding control group. Standard error propagation was used based on the SD of the group averages. The measured differences in ONL thickness between *Rs1h*-KO mice of neighboring age groups in the time-course study was statistically significant ($P < 0.01$, by ANOVA).

Discussion

Noninvasive imaging of the mouse retina can be a powerful tool for characterization of retinal degeneration. Imaging mice with the FD OCT system poses a different set of challenges than human retinal imaging. The FD OCT configuration for imaging humans typically uses a collimated beam of light incident on the eye, relying on the refractive elements of the cornea and lens to focus the beam on the retina. In our investigation, we found it preferable to cancel out the refrac-

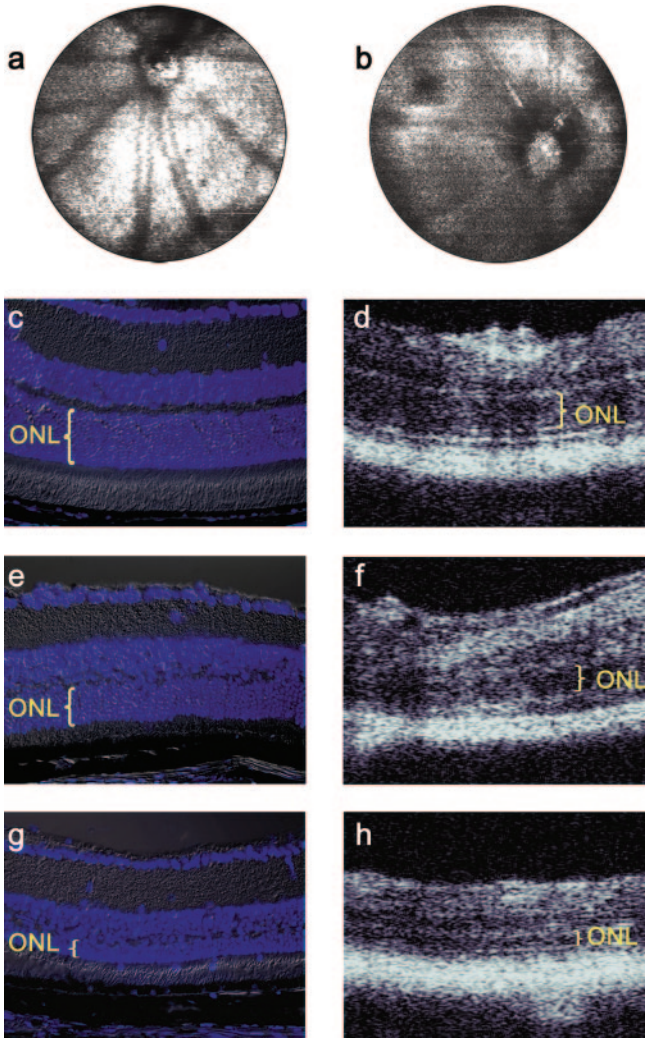

FIGURE 3. Fundus-type images reconstructed from FD OCT data acquired from (**a**) WT and (**b**) *Rs1h*-KO mice. DAPI-stained section and FD-OCT images from the same mice are shown for (**c**, **d**) 2-month-old WT, (**e**, **f**) 2-month-old *Rs1h* KO, and (**g**, **h**) 15-month old *Rs1h*-KO mice.

TABLE 1. ONL Thickness Measurements from *Rs1h*-KO Mice Obtained with FD OCT and DAPI-Stained Histology

	Measured Thickness							
	OCT		Histology		Ratio *Rs1h*/WT			
Month	μm	SD	Nuc.	SD	OCT	SD	Nuc.	SD
2	31.8	0.7	7.6	0.4	0.69	0.03	0.67	0.07
10	27.2	0.4	6.4	0.6	0.59	0.03	0.56	0.07
15	17.0	0.5	3.1	0.5	0.37	0.02	0.28	0.05

The ratio was calculated by using the ONL thickness of the control group. Nuc., number of nuclei counted from histology.

tion at the cornea with a contact lens and perform FD OCT imaging of the mouse eye using a converging beam.[12]

Comparison of the *Rs1h*-KO mouse retina images in Figure 3 with the WT counterparts indicates a marked difference in the retinal layer structure. Most noticeably, the OPL and IS/OS layers were not well defined in the FD OCT images of the *Rs1h*-KO mouse retina and appeared as broader regions of high scattering intensity. This appearance is consistent with earlier reports of histology in which the disruption of the cell layer architecture was notable in the OPL between the ONL and INL.[15]

In addition the disorganization of the retinal layers in the *Rs1h*-KO mice, superficial holes in the INL layer were also observed (Fig. 2d) as dark regions with no backscattered light signal. Since shadows of lower scattering intensity were not cast below the holes in the INL, we can conclude that the gaps must be full of a clear, nonscattering fluid. Similar results of holes in the INL had been observed in histologic samples of this strain of mice,[15] but because of the physical manipulation of the retinal samples in histologic preparation, it was not clear whether the gaps were due to delamination of the cell-to-cell contacts in the INL or the holes were present in the normal physiology. Because of the noninvasive nature of FD OCT imaging, we can conclusively confirm that the retinal holes in the ONL were not artifacts of histology. The holes observed in the FD OCT images of the *Rs1h*-KO mouse can also be compared with the observation of schisis cavities in the FD OCT images of humans with X-linked juvenile RS.[19–21] These images demonstrate that FD OCT has the potential to be used for noninvasive monitoring of the size and number of the retinal holes and provide feedback on the progress of retinal therapy without destroying the specimen.

Quantitative measurements of retinal degeneration were extracted from the data presented in Figure 3 to monitor the relative thickness of the ONL in the *Rs1h*-KO mice relative to WT mice. The averaged ONL thickness measurement of the *Rs1h*-KO mice obtained with the FD OCT and with histology is summarized in Table 1. The average thickness of the ONL in WT mice (independent of age) measured with FD OCT was 46 μm (SD 2; $n = 12$). The SD is less than the axial resolution of the system (~4 μm in tissue) and indicates a reasonable correlation of thickness measurements across all the animals and in both eyes. The average ONL thickness measurement in WT mice obtained by counting nuclei in the DAPI-stained histology was 11.4 nuclei (SD 1; $n = 10$), indicating an uncertainty of 9% in the WT mice.

The amount of retinal degeneration in the *RS1h*-KO mice relative to their WT counterparts is also summarized in Table 1. For 2-month-old mice, the FD OCT measurements indicated that the ONL in *Rs1h*-KO mice had degenerated to a mean of 69% (SD 3%; $n = 4$) of the WT ONL thickness. This measurement was statistically within experimental error of the same measurement made through histology. Further degeneration of the ONL was observed in the 10-month-old *Rs1h*-KO mice; with the FD OCT, the mean measured ratio ONL_{RS1h}/ONL_{WT} was 59% (SD 3%; $n = 4$). This measurement also agreed with the DAPI-stained histology measurements within experimental error. The mean measured ratio of ONL thickness in the 15-month-old *Rs1h*-KO mice relative to the WT was 36% (SD 2%; $n = 4$). However, because of the advanced degeneration of the ONL and severe disorganization of the retinal layers observed (Figs. 3g, 3h), delineation of the ONL thickness by FD OCT or DAPI-stained histology was nontrivial.

The thickness of the ONL in *Rs1h*-KO mice was measured for two additional age groups, 5 and 14 months. The histology measurements for these mice followed the trend observed in the other groups. The FD OCT measurements were used to graph the change in ONL thickness across the age groups; the data are presented in Figure 4a. The graph suggests that the retinal degeneration in *Rs1h*-KO mice is gradual between the ages of 2 months and nominally 1 year, at which point the rate of degeneration appears to increase.

The disorganization of the retinal layers in the *Rs1h*-KO mice made it difficult to establish definite boundaries of the ONL, which added to the uncertainty of the measurements. These problems were present in both the histologic and FD OCT measurements; however, the ability to average over multiple images with FD OCT presents a definite advantage of the noninvasive technique. An option to improve the repeatability

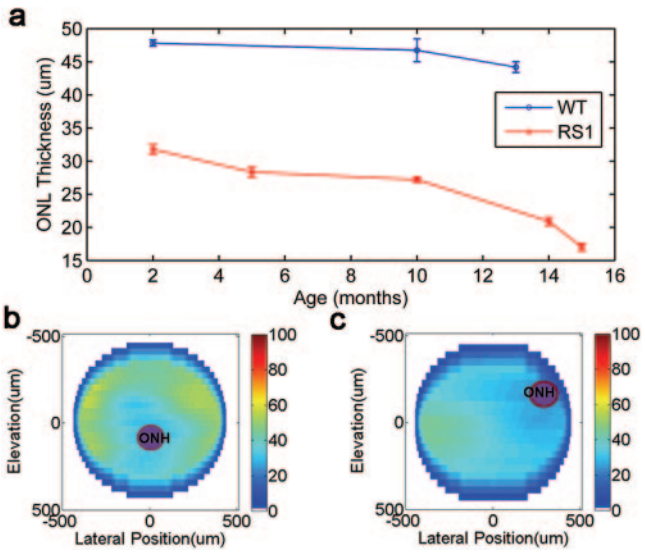

FIGURE 4. (**a**) ONL thickness of WT and *Rs1h*-KO mice measured with FD OCT in different age groups. Two-dimensional map of the ONL thickness for (**b**) WT and (**c**) *Rs1h*-KO mice at 2 months of age.

in the ONL thickness measurement would be to use automated segmentation software to eliminate human error and interobserver variation in the delineation of the ONL boundaries. With automated segmentation of the layers, the ONL thickness measurement with FD OCT can also be extended to a large area of the retina by processing the entire volume of data contained in the reconstructed fundus-type images shown in Figures 3a and 3b. Two-dimensional thickness maps of the ONL in a 2-month-old WT mouse and an age matched *Rsh1* KO mouse were processed and displayed in Figures 4b and 4c. Because of the manual labor necessary to segment the depth profiles in an entire volume, only every 10th elevation frame was extracted from the data to generate the thickness maps. In agreement with the results summarized in Table 1, the thickness maps in Figures 4b and 4c indicate that the ONL was thinner in the *Rs1h*-KO mouse than in the WT mouse. Automated segmentation of the retinal layers would benefit this application by providing higher spatial detail in the two-dimensional thickness maps by permitting processing of each acquired frame.

Conclusion

Noninvasive FD OCT imaging of the subsurface retinal layers was used to measure the thickness of the ONL in mice with retinal degeneration. In this study, we concentrated on the use of cost-effective and portable equipment for the FD OCT system. We compared the thickness measurements of the ONL in WT mice to thinning of the ONL in *Rs1h*-KO mice, the model for X-linked juvenile RS. Comparison of the noninvasive FD OCT measurements to histology demonstrated a strong correlation, and the measurement results matched within experimental uncertainty. At 2 months of age, the ONL layers in the *Rs1h*-KO mice had thinned down to nominally 70% of the WT thickness. By the age of 15 months, the thickness of the ONL layer in Rs1H-KO mice was nominally a third that of the WT. FD OCT also provided noninvasive images of the general disorganization of the retinal cell layers in the *Rs1h*-KO mice and was also able to image holes in the INL associated with the deficiency of retinoschisin.

References

1. Huang D, Swanson EA, Lin CP, et al. Optical coherence tomography. *Science.* 1991;254:1178–1181.
2. Fercher AF, Hitzenberger CK, Kamp G, Elzaiat SY. Measurement of intraocular distances by backscattering spectral interferometry. *Opt Commun.* 1995;117(1–2):43–48.
3. Cense B, Nassif N, Chen TC, et al. Ultrahigh-resolution high-speed retinal imaging using spectral-domain optical coherence tomography. *Optics Express.* 2004;12(11):2435–2447.
4. Wojtkowski M, Srinivasan VJ, Ko TH, Fujimoto JG, Kowalczyk A, Duker JS. Ultrahigh-resolution, high-speed, Fourier domain optical coherence tomography and methods for dispersion compensation. *Opt Express.* 2004;12(11):2404–2422.
5. Leitgeb RA, Drexler W, Unterhuber A, et al. Ultrahigh resolution Fourier domain optical coherence tomography. *Opt Express.* 2004; 12(10):2156–2165.
6. Bower BA, Zhao M, Zawadzki RJ, Sarunic MV, Izatt JA. Rapid volumetric imaging of the human retina in vivo using a low-cost, Fourier domain optical coherence tomography system. In: *Coherence Domain Optical Methods and Optical Coherence Tomography in Biomedicine IX*. San Jose, CA: SPIE; 2005:79–84.
7. Jiao SL, Knighton R, Huang XR, Gregori G, Puliafito CA. Simultaneous acquisition of sectional and fundus ophthalmic images with spectral-domain optical coherence tomography. *Opt Express.* 2005;13(2):444–452.
8. Drexler W, Fujimoto JG. State-of-the-art retinal optical coherence tomography. *Prog Retin Eye Res.* 2008;27(1):45–88.
9. Li QH, Timmers AM, Hunter K, et al. Noninvasive imaging by optical coherence tomography to monitor retinal degeneration in the mouse. *Invest Ophthalmol Vis Sci.* 2001;42(12):2981–2989.
10. Kocaoglu OP, Uhlhorn SR, Hernandez E, et al. Simultaneous fundus imaging and optical coherence tomography of the mouse retina. *Invest Ophthalmol Vis Sci.* 2007;48(3):1283–1289.
11. Horio N, Kachi S, Hori K, et al. Progressive change of optical coherence tomography scans in retinal degeneration slow mice. *Arch Ophthalmol.* 2001;119(9):1329–1332.
12. Srinivasan VJ, Ko TH, Wojtkowski M, et al. Noninvasive volumetric imaging and morphometry of the rodent retina with high-speed, ultrahigh-resolution optical coherence tomography. *Invest Ophthalmol Vis Sci.* 2006;47(12):5522–5528.
13. Ruggeri M, Wehbe H, Jiao S, et al. In vivo three-dimensional high-resolution imaging of rodent retina with spectral-domain optical coherence tomography. *Invest Ophthalmol Vis Sci.* 2007; 48(4):1808–1814.
14. Kim KH. Puoris'haag M, Maguluri GN, et al. Monitoring mouse retinal degeneration with high-resolution spectral-domain optical coherence tomography. *J Vision.* 2008;8(1):171–11.
15. Weber BH, Schrewe H, Molday LL, et al. Inactivation of the murine X-linked juvenile retinoschisis gene, Rs1h, suggests a role of retinoschisin in retinal cell layer organization and synaptic structure. *Proc Natl Acad Sci U S A.* 2002;99(9):6222–6227.
16. ANSI. *American National Standard for Safe Use of Lasers.* ANSI Z 136.1-1993; Orlando, FL: The Laser Institute of America; 1993: 7–43.
17. Sarunic MV, Asrani S, Izatt JA. Imaging the ocular anterior segment with real-time, full-range Fourier-domain optical coherence tomography. *Arch Ophthalmol.* 2008;126(4):537–542.
18. Zawadzki RJ, Leisser C, Leitgeb R, Pircher M, Fercher AF. *3D Ophthalmic OCT with a Refraction Correction Algorithm*. San Jose, CA: SPIE Biomedical Optics; 2003.
19. Apushkin MA, Fishman GA. Use of dorzolamide for patients with X-linked retinoschisis. *Retina.* 2006;26(7):741–745.
20. Apushkin MA, Fishman GA, Janowicz MJ. Correlation of optical coherence tomography findings with visual acuity and macular lesions in patients with X-linked retinoschisis. *Ophthalmology.* 2005;112(3):495–501.
21. Gerth C, Zawadzki RJ, Werner JS, Heon E. Retinal morphological changes of patients with X-linked retinoschisis evaluated by Fourier-domain optical coherence tomography. *Arch Ophthalmol.* 2008;126(6):807–811.